Back analysis of a building collapse under snow and rain loads in Mediterranean area

Isabelle Ousset[1], Guillaume Evin[1], Damien Raynaud[1], and Thierry Faug[1]

[1]Univ. Grenoble Alpes, CNRS, INRAE, IRD, Grenoble INP*, IGE, 38000 Grenoble, France. *Institute of Engineering and Management Univ. Grenoble Alpes.

Correspondence: Isabelle Ousset (isabelle.ousset@inrae.fr)

Abstract. At the end of February 2018 the Mediterranean area of Montpellier in France was struck by a significant snowfall that turned into an intense rain event caused by an exceptional atmospheric situation. This rain-on-snow event produced pronounced damage to many buildings of different types. In this study, we report a detailed back analysis of the roof collapse of a large building, namely the Irstea Cévennes building. Attention is paid to the dynamics of the climatic event, on the one hand, and to the mechanical response of the metal roof structure to normal loading, on the other hand. The former aspect relies on multiple sources of information that provide reliable estimates of snow heights in the area before the rain came into play and substantially modified the snow quality. The latter aspect relies on detailed finite element simulations of the mechanical behaviour of the roof structure in order to assess the pressure due to snow cover loading which could theoretically lead to failure. By combining the two approaches, it is possible to reconstruct the most probable scenario for the roof collapse. As an example of building behaviour and vulnerability to an exceptional rain-on-snow event in the Mediterranean area of France, this detailed case study provides useful key points to be considered in the future for a better mitigation of such events in non-mountainous areas.

1 Introduction

In the framework of snow falls, there are a number of reported cases of roof collapses caused by snow loads outside mountainous areas. The following events which occurred during the two past decades, and are for some of them reported in the scientific literature, can be mentioned:

- In France: collapse of the roof of a warehouse at Satolas-et-Bonce in the Isère department and of a supermarket store at Bricquebec in the Manche department (January 2010), several collapses of roofs in Western France (at least nine store roofs in the Manche department) in March 2013, several damage to shops in the department of Hérault at the end of February 2018 in the cities of Béziers, Lattes, Montpellier, Peyrols (see examples shown in Figure 1).
- In Europe: collapse of a self-weighted metallic roof in Spain in March 2004 (del Coz Díaz et al., 2012), collapse of a public fair pavilion in Italy during February 2001 (Brencich, 2010), total collapse of the Katowice fair building in Poland which caused 65 deaths and 180 injuries in January 2006 (Biegus and Rykaluk, 2009), collapse of the Bad Reichenhall Ice Rink roof in Germany which led to 15 deaths the same month (Winter and Kreuzinger, 2008), collapse

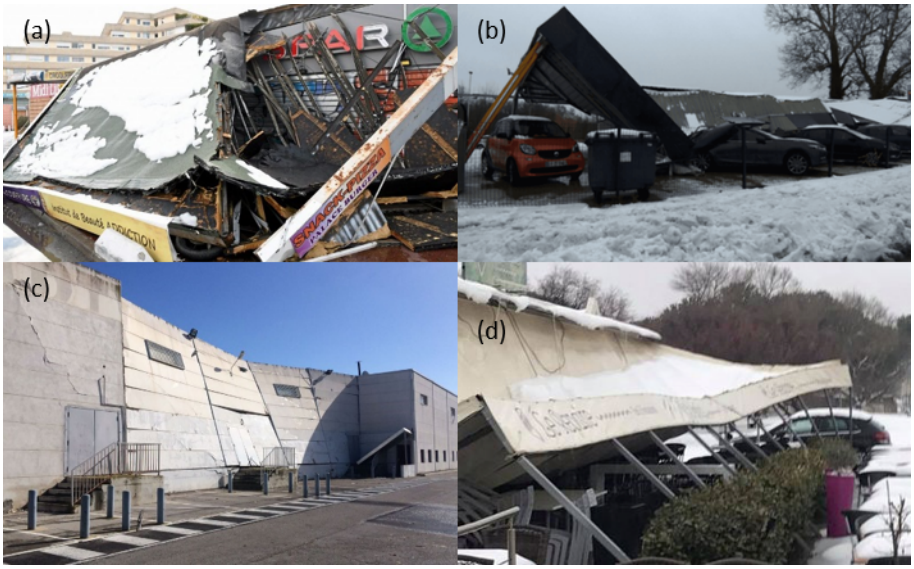

Figure 1. Roof collapses due to heavy snowfalls occurred on 28 February and 1st March 2018 in the surroundings of Montpellier, France: collapses of (a) the shopping center Estanove in Montpellier (Photo credit: ©Jean-Michel Mart), (b) a car wash station in Lattes (Photo credit: ©Le Petit Journal de Lattes), (c) the Darty store in Peyrols (Photo credit: ©France 3 LR / S. Banus) and (d) a restaurant in La Grande Motte (Photo credit: ©France 3).

of a gymnasium roof in Switzerland in 2009 (Piskoty et al., 2013), collapse of a store hall in Gdansk (Poland) in February 2010 (Biegus and Kowal, 2013), collapse of a shopping facility in Poland during January 2015 (Krentowski et al., 2019).

– In other regions of the world: collapse of truss roof structures in Turkey in February 2003 (Caglayan and Yuksel, 2008) as well as during January and October 2015 (Piroglu and Ozakgul, 2016; Altunişik et al., 2017), many roof collapses in Northeastern United States (O'Rourke and Wikoff, 2014) during the winter 2010-2011.

The principal source of explanation given for the various buildings' collapses that were induced by snow loads, and were reported in the recent above-mentioned literature, generally relies on a stronger (greater than the standard) snowfall hazard (Strasser, 2008; Holický and Sýkora, 2009; Geis et al., 2012; Le Roux et al., 2020). It should be noted that a poor design or insufficient material strengths may sometimes be identified as another main reason for the collapse (Biegus and Rykaluk, 2009; Caglayan and Yuksel, 2008; Brencich, 2010; del Coz Díaz et al., 2012; Biegus and Kowal, 2013; Piskoty et al., 2013; O'Rourke and Wikoff, 2014; Altunişik et al., 2017; Krentowski et al., 2019). In a large meta-analysis of building failures related to snow loads, Geis (2011) found that these incidents are commonly attributed to the large amount of snow, followed by problems in the design of the building, melting snow and rain-on-snow events.

The current paper reports a detailed and specific case study of a roof collapse induced by a rain-on-snow event which occurred in the Mediterranean area and concerned a scientific laboratory which belonged to the Irstea (now INRAE) French

research institute. This is one of the several roof collapses which occurred in this area at the end of February 2018 (see Figure 1).

Careful attention is paid to two important questions which are tackled independently in a first step: what was the maximum load admissible by the building before the event? And what was the maximum load exerted by the snow cover on the roof at the moment of the roof collapse? The first question is particularly delicate , especially because of the highly non-linear mechanical behaviour of the complex structure involved, and some uncertainty about the initial state of the structure before the event. It will be addressed in Section 3 thanks to detailed numerical simulations based on the finite element Abaqus software (Dassault Systèmes, 2017). The second question is complex too, in particular because the meteorological event consisted of a snowfall followed by rain at the time of the roof collapse. This question will be tackled in Section 2 thanks to multiple sources of information: outputs from the AROME numerical model, which is the French fine mesh numerical weather forecast service model, social network testimonies and weather observations. In a second step, by making the link between the analysis of the snow and rain hazard (Section 2) and the modelling of the mechanical behaviour of the building subject to a uniform pressure field that roughly mimics snow-induced loading (Section 3), a detailed analysis of the most probable scenario for the roof collapse of Irstea Cévennes building is proposed in Section 4. This example of a roof collapse caused by an intense rain-on-snow event which occurred in the Mediterranean area is finally used in the discussion section to emphasize a number of questions which need to be addressed in the future, in particular what evolution is expected about the characteristic snow loads in non-mountainous areas in a context of climate change and what improvements can be proposed to minimize the risk of a roof collapse due to snow loading in those areas.

2 Description of the meteorological event

2.1 An exceptional atmospheric situation

At the end of February 2018, France, and more generally Europe, was subject to wintry weather conditions. A disordered polar vortex unleashed a very cold air mass through central Europe around 24-25 Feb. Driven by a powerful anticyclone localized in Scandinavia and a sustained eastern flux, this cold spell spread over western Europe during the following days, resulting in the most intense cold spell over Europe since Feb. 2012 which is referred to as “Beast from the East”.

Figure 2 presents the outputs of the high-resolution AROME model for different times and lead times. The regional AROME model assimilates various types of observations (radar, ground measurement data, radio, satellites radiances (see Bouttier and Roulet (2008)) and must be interpreted with care. AROME outputs provide interesting information regarding the spatio-temporal dynamics of the meteorological event. Four parameters are represented: temperature at 850 hPa, temperature at 2 m, wind at 10 m and precipitation amount accumulated in 1 hour.

This event can be described as follows:

– **28/02/2018 08:00 - Formation of a convergence zone:** On the 28th of Feb., at 8 am (local time), just before the beginning of the snow storm, temperatures are very cold over lands in the region, in altitude ($-6°$ at 850 hPa, corr.

to about 1500 m) and on the ground (between $-2°$ and $6°$ at 2 m). We can observe a line of convergence on the sea, with, on the one side, cold air brought from the North-East related to the cold spell and, on the other side, winds from the South-East bringing warm air. This convergence zone will generate vertical fluxes and will create this atmospheric disturbance at the origin of important snow and rain accumulations.

- **28/02/2021 14:00 - Beginning of the snowfall:** At 2 pm (local time), important precipitation amounts occur around the convergence zone, mainly along the coast but also offshore. At the North-West of this zone (Montpellier, Béziers), despite of a slight and progressive increase of temperature at the ground and in altitude, the supply of cold air from the North leads to solid precipitation only.

- **28/02/2018 20:00 - Snow/rain event:** Between 8 pm and 2 am (local time), winds from South-East intensify and precipitation amounts on Montpellier increase. AROME model shows a temporary movement of the convergence zone from the plains. Then, a North-East flux with cold air at low altitudes leads to snow again in the surroundings of Montpellier.

- **01/03/2018 02:00 - Warming and rainfall gets stronger:** During the night between $28/02/2018$ and $01/03/2018$, warming is rising at high altitudes (from $-3°$ at 6 pm to $0°$ at 2 am at 1500 m) and rainfall becomes dominant.

- **01/03/2018 08:00 Intense rain event:** In the morning of $01/03/2018$, despite of the persistence of the convergence zone and cold ground temperatures, warming in altitude is too important and precipitation only falls as rain.

2.2 An intense rain-on-snow event

This rain-on-snow event is exceptional in the region of Montpellier considering the accumulated amount of precipitation and the amount of precipitation fallen as snow. Ground measurements indicate that snow depth of more than 25 cm have occurred only five times since the 1950s (35 cm in February 1954, 35 cm during the winter 1962-1963, 27 cm on the 14-16/01/1987, 28 cm on the 22/01/1992 and the event described here). The empirical return period of the snow event alone exceeds 10 years (five events in 70 years). What makes the rain-on-snow event exceptional is the large amount of rainfall which followed the snow event. Its occurrence can be explained by the main following elements:

- the presence of very cold air at all altitudes and in particular at the low troposphere;
- the blocking of a strong convergence zone leading to an intense rain/snow event;
- the preservation of this convergence zone and cold wind supply from the North-East around Montpellier.

Figure 3 presents the evolution of the type of precipitation simulated by the AROME model for 1h lead time. AROME clearly simulates an intense snow event from 28/02/2018 at 14:00 until the end of this day, followed by a rain/snow event during the night. An intense rain event brings high liquid precipitation during the whole day of 01/03/2018.

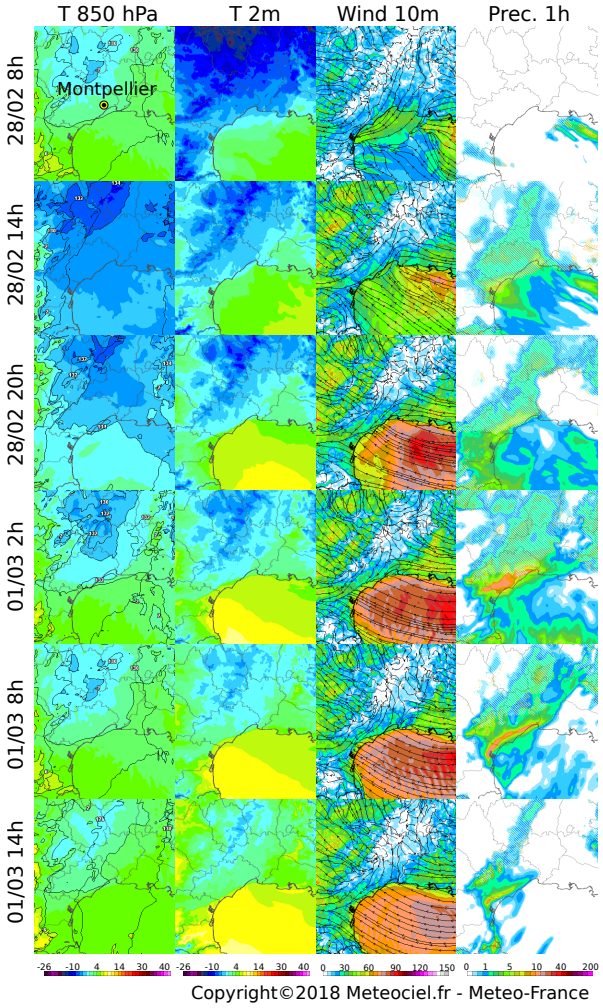

Figure 2. Outputs of the high-resolution AROME model for the following parameters: temperature at 850 hPa [°C], temperature at 2 m [°C], wind at 10 m [km/h] and precipitation amount accumulated in 1 hour [mm]. The maps shown on each line correspond to different runs for 1h lead time, from 28/02 at 8:00 to 01/03 at 14:00 (local time). Source: Meteo-France.

2.3 Snow accumulation

Meteo-Languedoc is an association providing various information about weather forecasts and natural risks on the region around Montpellier. This exceptional data is described in details on their website (https://www.meteolanguedoc.com/evenements-majeurs-en-lang episode-neigeux-du-28-fevrier-2018-jusqu-a-35-cm-pres-de-montpellier/p513, last access: 24 January 2022) and includes various information about the meteorological event, including photos from amateurs following their facebook page (https://fr-fr.facebook.com/MeteoLanguedoc/, last access: 24 January 2022). Through their facebook page, MeteoLanguedoc asked their 120 000 fol-

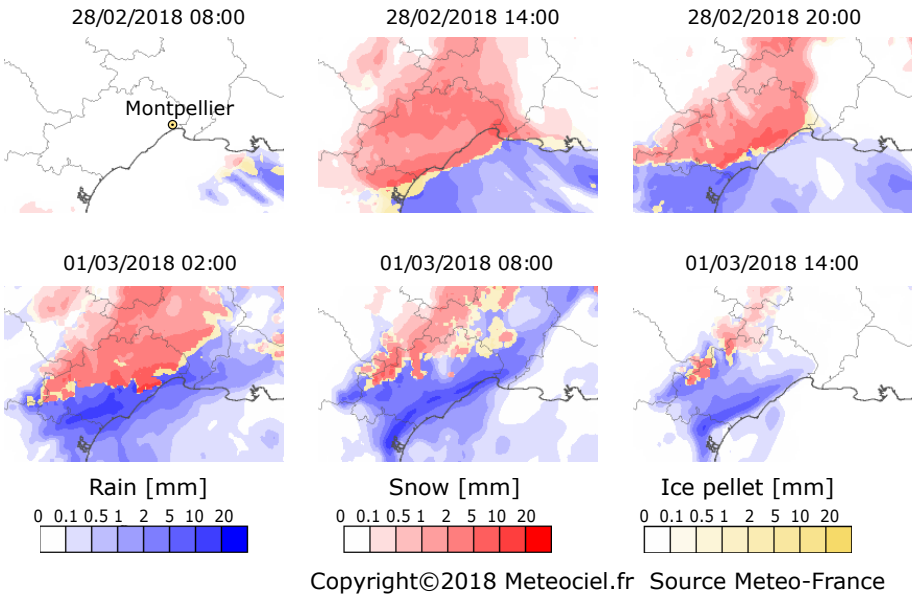

Figure 3. Outputs of the high resolution AROME model for the type of precipitation, for 3 runs at 1h lead time (local time is indicated). Source: Meteo-France.

lowers to provide observations, and photos supporting these observations. Thanks to the collection of 5 000 feedbacks, a robust estimation of the depth of the snowpack at the end of the snow event was obtained, leading to the interpolated field of snow accumulation provided in Figure 4. The data clearly shows that the snow depth was more important at the North of Montpellier, likely due to a hill separating the city center from the Lavalette site.

2.4 Estimation of the snow height and density at the time of the collapse

Figure 5 shows the evolution of the temperature, rain and snow amounts according to two different and independent sources of information:

- Just next to the center of Irstea in Montpellier, a weather station (the Lavalette station) records various meteorological parameters, including temperature and rain. For this station, the tipping-bucket rain gauge is not heated and snow was probably blocking the rain gauge according to the operator of the station.
- SAFRAN reanalysis (Vidal et al., 2010) provides weather parameters at a resolution of 8 km over France, using a dense gauge network. However, this network does not include the station at Lavalette.

Both sources of information clearly show the increase of temperature from the morning of 28/02/2018 until the building collapse. SAFRAN reanalysis records an accumulation of snow water equivalent of 35 mm followed by 58 mm of rainfall before the collapse, with a rain/snow transition during the night between 28/02 and 01/03. The rain gauge, which might have underestimated the rainfall accumulation due to the presence of snow in the receptacle, records 45 mm.

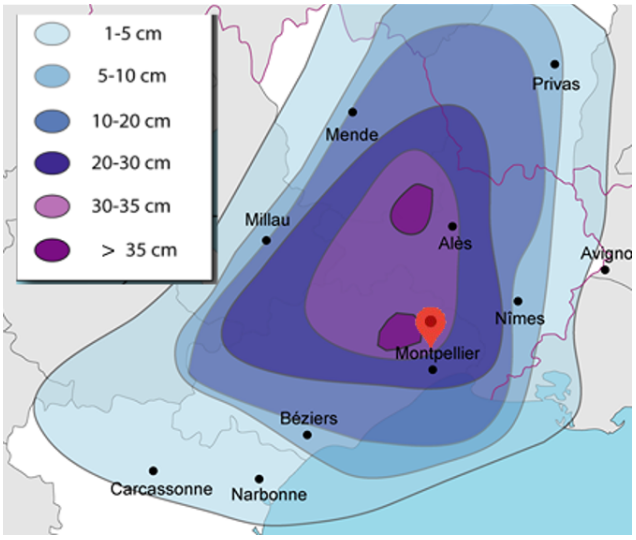

Figure 4. Snow accumulation during the snow event of 28/02/2018, based on 5000 testimonies. Source: Meteo-Languedoc.

The different sources of information (outputs from AROME model, social network testimonies, weather data) on the snow and rain event lead to the following scenario. It can be considered with little uncertainty that the snow depth in the area was between 30 cm and 35 cm, on a cold ground. Since the Irstea building was located right next to the 30 cm curve (see Figure 4), 30 cm is considered as the best estimate, but there is an uncertainty around this estimate.

The snow was having a density in the range of 250 kg.m^{-3} before the rain event, based on the fact that most of the Facebook testimonies reported a heavy snow type, which is typical of a Mediterranean area. A rain-snow transition limit is then derived from available measurements, the vertical profile of temperature, and other available information. The snowpack has been filled by 50 to 60 mm of rainfall, noting that the drainage system (see Figure 9 given in Section 3) was probably blocked by the snowpack already present on the roof at the beginning of the rain event, and that water was mostly stocked on the roof. More details on this crucial point will be given in Section 4. In light of these different sources of information and considering the additional weight provided by water from the rainfall, we can roughly estimate that the very wet snowpack on the roof easily reached a high density around 600 kg.m^{-3} at the time of the collapse, which occurred on March 1 at around 6 pm.

The ability of a snowpack to absorb water largely depends on its initial porosity and the boundary conditions of the problem. Very loose snow, like dry and cold fresh snow ($50 - 100$ kg.m^{-3}), can quickly absorb a large amount of water in just a few hours. In contrast, denser snow, particularly if already wet such as the one likely involved in the event discussed in this study, may have a more limited capacity to absorb water (Marshall et al., 1999). In the former case, water will follow preferential paths and accumulate in specific areas at the bottom. Under natural conditions (open system), with constant water circulation and a homogeneous snowpack, densities higher than $300 - 400$ kg.m^{-3} are not expected over a typical daily period (Marshall et al. (1999), figure 2). However, if boundary conditions prevent water evacuation (closed system) and depending on the amount of water available (intensity of the rain event until building collapse), higher ultimate densities can be expected, which correspond

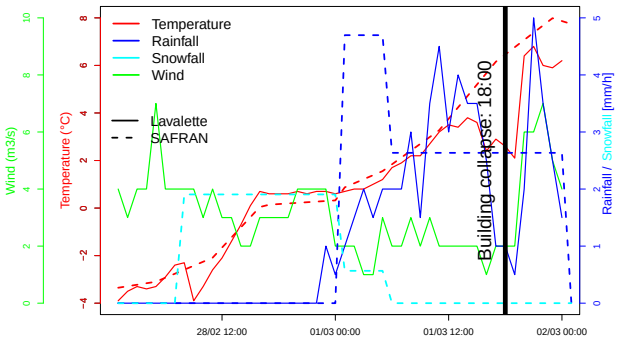

Figure 5. Weather observations at the station of Lavalette (plain lines) and SAFRAN reanalysis at the grid point covering Irstea building (dotted lines).

to an equivalent mean density for the mixture of wet snow (in some zones) and water (in other zones). In the present case, the wet snowpack was probably heterogeneous with zones of soared snow at higher density ($300 - 400$ kg.m^{-3}) than the initial snow (250 kg.m^{-3}) and other zones at the bottom with accumulated water (1000 kg.m^{-3}) due to preferential water flows. The assumed value of 600 kg.m^{-3} used in this study for ultimate snow density corresponds to an equivalent value that defines the (equivalent) pressure exerted by the combination of snow and rain accumulations.

As the entire site was evacuated in the early afternoon of March 1, only the caretaker was present at the time of the building collapse, but he did not observe the snow on the roof. Consequently, there is no information available regarding the depth and distribution of the snow on the roof. Given that the wind was only at Force 1 with a velocity between 1 and 4 m.s^{-1} during both days, it is unlikely that the wind could have had an effect on the distribution of snow on the roof and on the collapse of the building.

3 Modelling of mechanical behaviour of the loaded building

3.1 Description of the building

3.1.1 Initial state (before collapse)

The Cévennes building was an experimental hall built in 1982 and situated at Lavalette domain in Montpellier (see Figure A1 in Appendix A). At the time of its failure, it sheltered a wind tunnel and a mezzanine built in 2014 along the northern facade, as well as offices on two levels along the southern facade. Figure 6 gives an overview of the Cévennes building before damage. Its dimensions on the ground were 40.5 m in the east-west direction and 49 m in the north-south direction (area of almost 2000 m^2) and 10 m high.

The supporting structure of the building consisted of three-dimensional vertical metallic trusses designed to support the flat roof (see an example shown in Figure 7a) and themselves supported by metal tubular pylons that were arranged along the

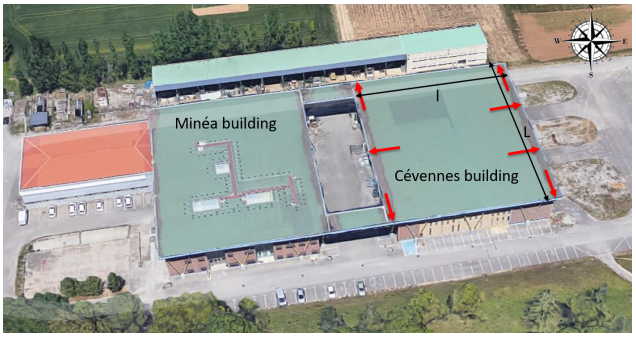

Figure 6. Overview of the Irstea Cévennes building before damage, with drainage points of rainwater indicated by red arrows (Photo credit: ©Google Earth 2014, adapted by I. Ousset).

Figure 7. View of the supporting structure of the Irstea Cévennes building before its damage: (a) red-colored roof metal frame and (b) supporting tubular pylons (in yellow) along the facades.

facades of the building. The lattice structure, consisting of elements welded or bolted together, extends over the entire roof surface and withstands all the forces acting upon it. For the southern, western and northern facades of the building, the tubular pylons consisted of two round tubular profiles arranged in V-shape and sealed on concrete blocks anchored in the ground (see photograph on Figure 7b, and sketches on Figures 8a and 8b). For the eastern facade of the building, they consisted of rectangular tubular profiles and a Saint Andrew's cross obtained with T-profiles (see sketch on Figure 8c). It is worth noting here that no such tubular pylons had been settled inside the building in order to allow the movement of large-size vehicles, such as agricultural tractors.

The roof had a slight slope of 1 % on each side of a peak line oriented north south, which allows rainwater to flow towards the east or west of the building and drain through 20 cm high outlets located at the base of the low walls on the roof edges, as shown in Figure 9. There were four outlets at the ends of the north and south edges, one in the middle of the west edge, and two at the quarter and three-quarter points of the east edge, as indicated by the red arrows in Figure 6.

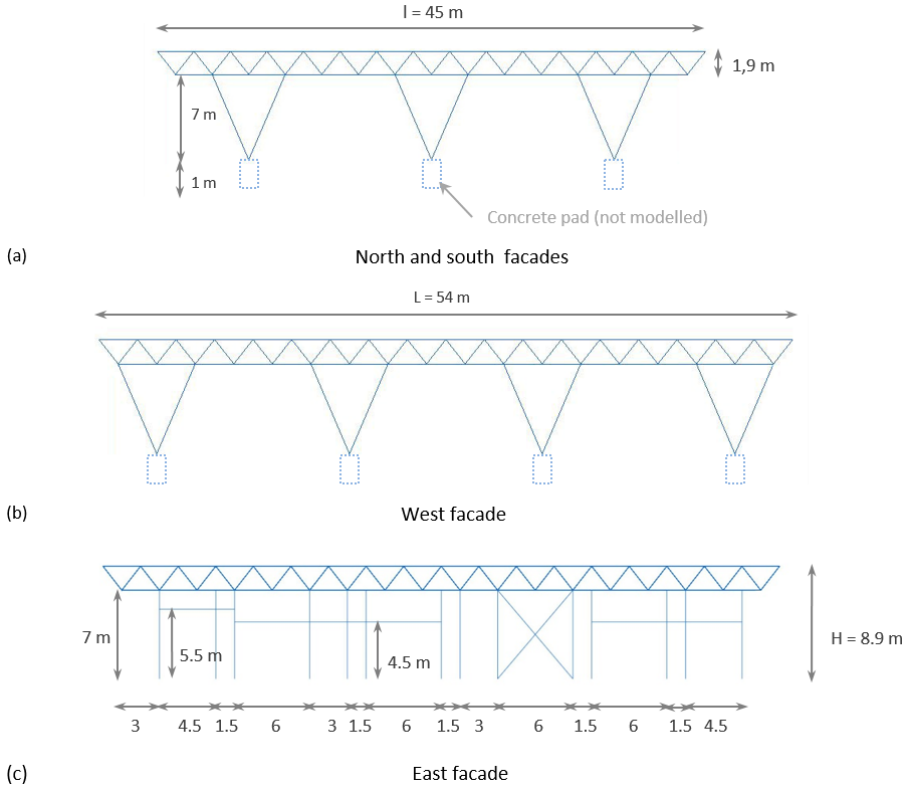

Figure 8. Sketches showing the geometrical details (size and shape) of the metallic structure of every facade of the Irstea Cévennes building.

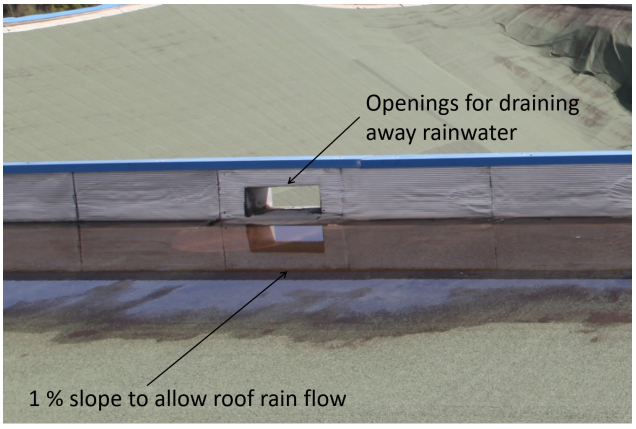

Figure 9. Close-up view of the roof rain drainage system of the Irstea Cévennes building.

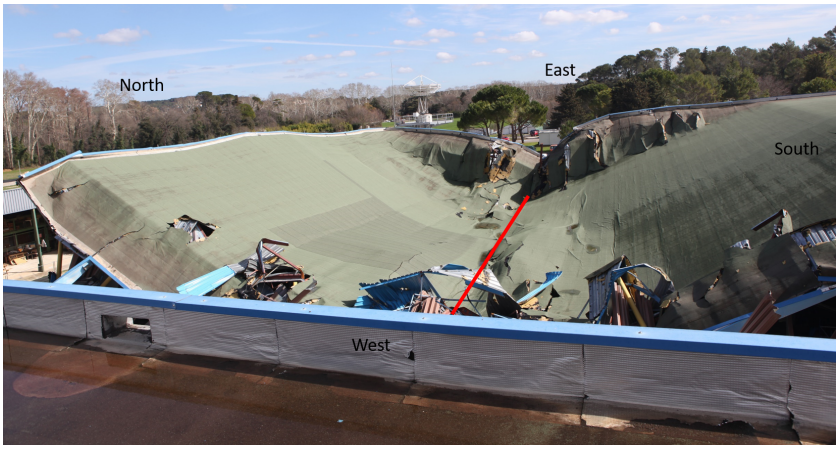

Figure 10. Overview of the damaged Irstea Cévennes building.

3.1.2 Damage observed (after collapse)

This section gives a brief summary of the main damage observed during a field visit on 18 March 2018. Additional details are provided in Appendix A. The snow load led to the collapse of the experimental hall of the Irstea Cévennes building in the central part of the structure, in the west-east direction, as seen by the red line in Figure 10. The western and eastern facades were heavily damaged, as seen in Figs. 11a and 11c. On the contrary, the other two facades (see Figure 11b and 11d) were much less damaged due to the presence of the inner concrete walls of the offices and of the inner metal frames of the laboratory rooms along the south and north facades, respectively.

Local damage observed on structural elements consist in (i) buckling and bending for the roof tubular profiles, (ii) bending and shear for the tubular supporting pylons and (iii) cracking for the offices' walls. Close-up views of those damage are shown in Figure A2.

3.2 Description of the finite element model

In order to investigate in detail the mechanical response of the Irstea Cévennes building and thus better understand its collapse under snow and rain loading, the metal supporting structure was modelled using the Finite Element (FE) Abaqus software (Dassault Systèmes, 2017). Figure 12 shows an overall sketch of the modelled structure with respect to the description of the building provided in the previous subsection. The details of the roof metal frame which was fully modelled by the FE Abaqus are shown in Figure A3. The dimensions of the structure and of all its components are given in Table A1.

The structure is modelled in Abaqus by 132 778 Timoshenko beam elements of B31 (two-node linear beam element in space) type and 0.05 m long.

The Irstea Cévennes building dates back to the 1980s, and as such, obtaining exact design records has proven to be very difficult. The type of steel used for the supporting structure is therefore unknown, and no material testing was carried out after

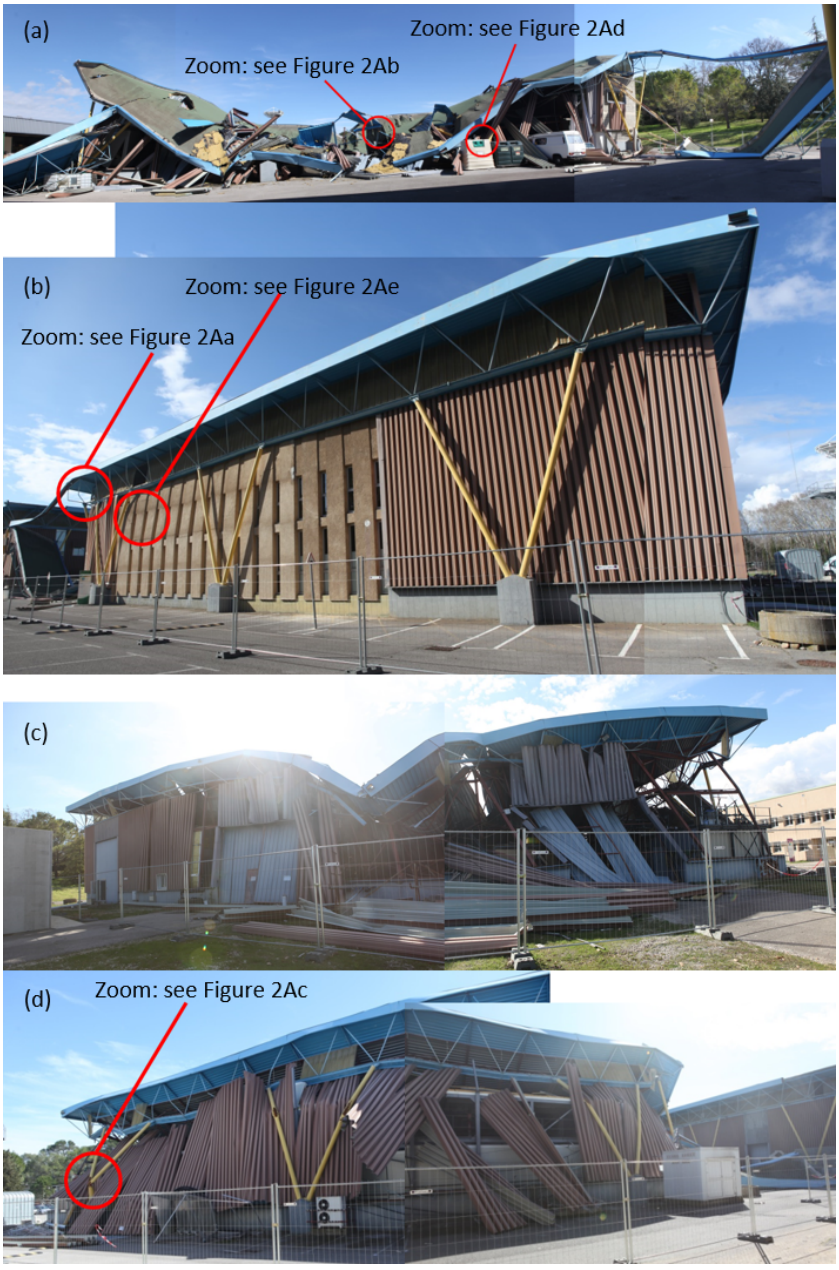

Figure 11. Different pictures showing the hierarchy of damage as observed on 18 March 2018 on western (a), southern (b), eastern (c) and northern (d) facades of the Irstea Cévennes building.

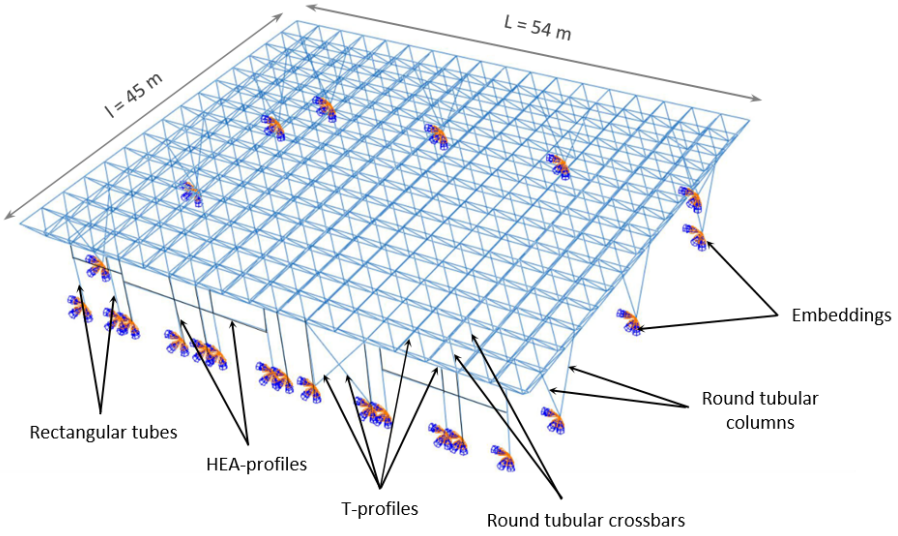

Figure 12. Overview of the metal structure of the Cévennes building modelled with the FE Abaqus software.

Table 1. Material characteristics considered in the FE model for describing the behaviour of the entire structure.

Parameter	Notation	Unit	Value
Type	S235	-	-
Density	ρ_s	kg.m^{-3}	7850
Young modulus	E_y	MPa	210000
Poisson ratio	ν	-	0.3
Yield strength	f_y	MPa	294
Ultimate strength	f_u	MPa	432
Ultimate strain	ε_u	-	0.2

the collapse. It is assumed that the supporting structure was made entirely of S235 steel, which is commonly used in building construction. The steel behaviour is described by a linear elasto-plastic law with strain hardening that involves four parameters: the Young modulus E_y, the yield strength f_y, the ultimate strength f_u and strain ε_u. Their numerical values used in the FE simulations are provided in Table 1. In the absence of tests carried out on steel elements after the collapse, mean values of steel strengths were used in the FE model based on the new Eurocode for design of steel structures: f_y = 1.25 x 235 = 294 MPa and f_u = 1.2 x 360 = 432 MPa, along with an ultimate strain ε_u = 20 % .

Two pressure fields corresponding to the dead weight of the sheet covering the lattice structure and the snow-induced loading are taken into account. They are reflected in the model by line forces applied over the total upper T-profiles of the roof. Values of these line forces, identified in Table 2 and 3, depend on whether the T-profile is located on the perimeter of the lattice or

inside and on the choice retained for the distribution of the snow pressure field. The uniform pressure due to the dead weight of the sheet is taken equal to 60 N.m^{-2}. The distribution of snow load can vary over time based on the deflection observed on the lattice roof and its interaction with the dynamics of the snow cover. We believe that the distribution of the initial snow load (before rainfall) was nearly uniform due to the low slope of the roof and the light wind during snowfall. Then, rain likely first accumulated on the west and east edges of the roof until the direction of the slope of the roof changed due to an increase in deflection (i.e. when the deflection of the roof became too important and counter-balanced the initial 22.5 cm roof height). All the rainwater is assumed to have remained on the roof until the building collapsed because the outlets were blocked by snow. After that, rainwater accumulated in the center of the roof. Therefore, three different cases of pressure distribution were studied, as shown in Figure 13: a uniform distribution, a case where water rapidly flowed on the edges of the roof, and a case where water mainly accumulated in the center of the roof. In the case of a uniform distribution, the pressure mimicking snow load varies between 0 and a maximum pressure of 4905 N.m^{-2} (Table 2), which corresponds to a two-meter high snowpack with a density of 250 kg.m^{-1} or a one-meter high wet snowpack with a mean density of 500 kg.m^{-1}. In the other two cases, snow-and-rain line loads applied to the structure after rainfall are identified in Table 3 based on the location of the T-Rebars mentioned in Figure 14.

The dead weight of the structure is also taken into account, considering a steel density of 7 850 kg.m^{-3} (see Table 1).

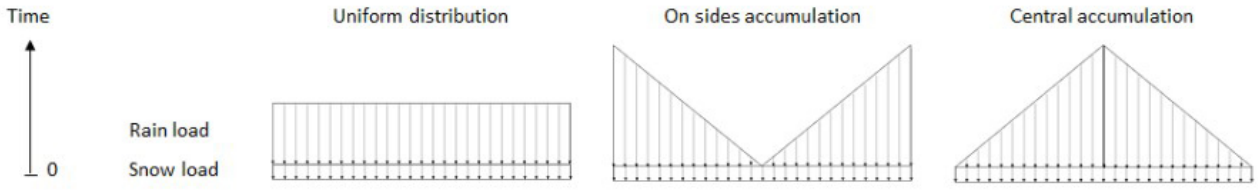

Figure 13. Three different assumptions made for the distribution of snow and rain loads on the roof.

No wind loads were taken into account in this study, as wind effects were deemed negligible on the day the structure collapsed.

Since the roof frame elements are not hinged in the real structure, the roof frame has been modelled in one piece with rigid connections between elements. The links between the roof frame and the supporting tubular pylons are actually of a pivot type in the direction parallel to the facades to withstand the wind. Since the loads taken into account in the FE model are all vertical, this hinge is not supposed to be applied. A FE model with pivots has however been tested; both models led to similar results. A rigid linkage between these elements has therefore been taken into account in the model. To finish, all the columns of the facades are embedded.

Table 2. Applied line loads to the structure during the pushover FE simulations in the case of a uniform distribution.

Location of the T-profile	Roof weight [N.ml^{-1}]	Snow-and-rain weight [N.ml^{-1}]
Roof perimeter	45	0 to 3679
Inside the roof	90	0 to 7358

Table 3. Snow-and-rain line loads [N.ml^{-1}] applied to the structure during the pushover FE simulations in the case of pressure distribution with accumulation on the sides and central accumulation.

	Accumulation on the sides			Central accumulation		
T-profile rebars location	NS	WE ext	WE int	NS	WE ext	WE int
A	6867	6867	13734	490.5	490.5	981
B	12753	5886	11772	1962	1471.5	2943
C	10791	4905	9810	3924	2452.5	4905
D	8829	3924	7848	5886	3433.5	6867
E	6867	2943	5886	7848	4414.5	8829
F	4905	1962	3924	9810	5395.5	10791
G	2943	981	1962	11772	6376.5	12753
H	1226.25	245.25	490.5	13488.75	7112.25	14224.5

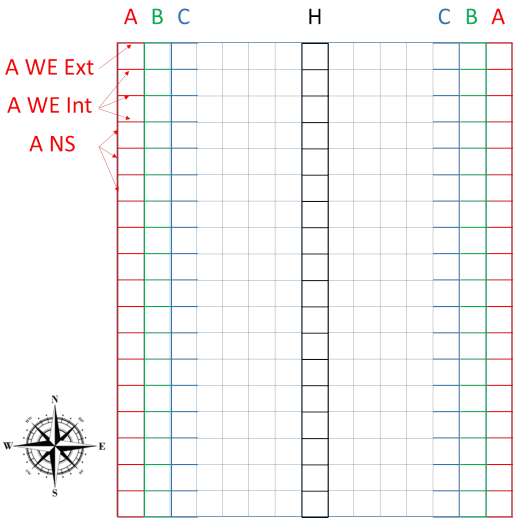

Figure 14. Location of the T-rebars affected by snow-and-rain loading.

3.3 FE simulations' results

It is important to stress here that one difficulty may arise from the fact that the initial state of the building before the event is known with some uncertainty. In particular, past damage may have already occurred before the event of 2018 and altered the initial integrity of the structure.

In fact, even though the studied building is not located in an area with intense snow events, it had to support heavy loads (at least) three times in the past since its construction:

- around 27 cm on January 14-16, 1987;
- around 28 cm on January 22, 1992;
- less than 10 cm on March 7, 2010.

To our knowledge, no survey has been conducted on the structure of the Cévennes and Minéa buildings between the date of their construction and the 2018 incident. Following this event, only a technical opinion of the strength of the adjacent Minéa building was requested. This report concluded that the overall strength of the structure was satisfactory, but a number of points requiring vigilance were identified:

- significant stagnation of stormwater on the roof;
- slight buckling and traces of corrosion on some profiles (angles and tubular profiles) at the level of the roof metal frame;
- buckling on one of the profiles of a Saint-Andre's cross;
- V-columns in satisfactory condition, with slight corrosion at the head and anchor plate;
- cracks and chips with visible reinforcement in concrete blocks used for anchoring the V-columns.

Given the limited information available on previous events and any damage that may have resulted from temporary loads applied to the structure in the past, this study has not taken into account any such deterioration of the structure.

However, it is worth noting that no modifications were made to the supporting structure from the time of its construction to the time of its collapse. The only changes made were interior fittings (mezzanines supported by the ground) in 2014.

Firstly, quasi-static pushover tests carried out by varying the pressure due to snow load. They can lead to the failure of the supporting structure, considering the different following criteria.

The first two failure criteria considered correspond to the attainment of two stresses states: (i) an accumulation of stresses equal to the yield strength of steel in a certain part of the model, which causes the elastic model to diverge (yield limit) and (ii) an accumulation of stresses equal to the ultimate strength of steel, causing the elasto-plasic model to diverge (ultimate limit). These criteria indicate the onset of deterioration that could potentially have a significant impact on the structure.

Two other failure criteria are based on the next two beam deflections: (iii) the vertical displacement equal to $l/200 = 0.225$ m and (iv) the vertical displacement equal to $L/200 = 0.27$ m and another one is (v) the maximum horizontal displacement at the top of the columns equal to $H/150 = 0.047$ m.

Secondly, a non-linear buckling analysis was performed in two steps:

- a linear buckling analysis was conducted to obtain the first fourteen buckling mode shapes of the structure and their corresponding eigenvalue buckling loads. This analysis was carried out by applying a vertical snow pressure of 1 Pa, after a static step that accounted for the dead load of the structure;

- a non-linear buckling analysis (using the static Riks procedure) of the FE model was conducted, integrating geometric imperfections corresponding to the displacement results of the pre-buckling analysis, in order to estimate the critical bifurcation snow pressure. Only the first mode shape was taken into account, and the corresponding displacements were multiplied by an argument equal to 1 % of the crossbars thickness, *i.e.* 0.5 mm, which corresponds to the manufacturing tolerance value of a round tubular profile with an outside diameter of less than 75 mm.

This analysis allowed to obtain (vi) the first linear buckling load and (vii) the bifurcation buckling load that causes the actual buckling, taking into account the geometric imperfections.

Table 4 presents the (snow-and-rain) load values that result in structural failure according to the different failure criteria for the three assumptions of snow loads distribution on the roof. They typically range between 645 and $3\,410$ N.m^{-2} depending on the selected failure criterion and the assumption of pressure field distribution. The beam deflection and elastic criteria provide intermediate failure pressure values between the lowest and the highest values obtained from the buckling criterion and the ultimate limit or horizontal displacement criterion, respectively. However, for non-uniform snow pressure fields, the ultimate limit is not reached due to code divergence.

The snow loads that cause buckling, as obtained from the FE simulations, are similar regardless of the distribution of the snowpack. This is because the load that causes buckling (645 kN.m^{-2}) is lower than the pressure exerted by a uniform snowpack of 30 cm thickness (which is 735 kN.m^{-2}). However, when considering other criteria, the case of a central accumulation of snow always proves to be the most critical.

Table 4. Snow load values leading to the failure of the supporting structure for the different criteria.

Failure criteria	Snow load value $[N.m^{-2}]$		
	Uniform distribution	Accumulation on the sides with 30 cm of uniform snowpack	Central accumulation
Yield limit	1 330	1 345	1 325
Ultimate limit	3 410	Not reached (Code divergence)	Not reached (Code divergence)
$y_{max} = 0.225$ m	1 360	1 660	1 205
$y_{max} = 0.27$ m	1 660	2 090	1 415
Horizontal displacement	2 350	Not reached	1 915
Linear buckling	935	930	940
Non-linear buckling	645	645	645

Table 5. Results of the eigenvalue buckling analysis of the structure.

Eigenvalue mode	Corresponding load [N.m^{-2}]	Corresponding displacement [m]	Location of the buckling crossbars
1	934.6	1.373	West facade
2	937	1.366	West facade
3	939	1.279	West facade
4	941.1	1.277	West facade
5	1051.3	1.241	East facade
6	1055.5	1.392	East facade
7	1099.6	1.318	East facade
8	1105.2	1.353	East facade
9	1271.2	1.385	West facade
10	1277.2	1.247	West facade
11	1277.8	1.387	West facade
12	1283.7	1.244	West facade
13	1293.5	1.184	West facade
14	1298.4	1.184	West facade

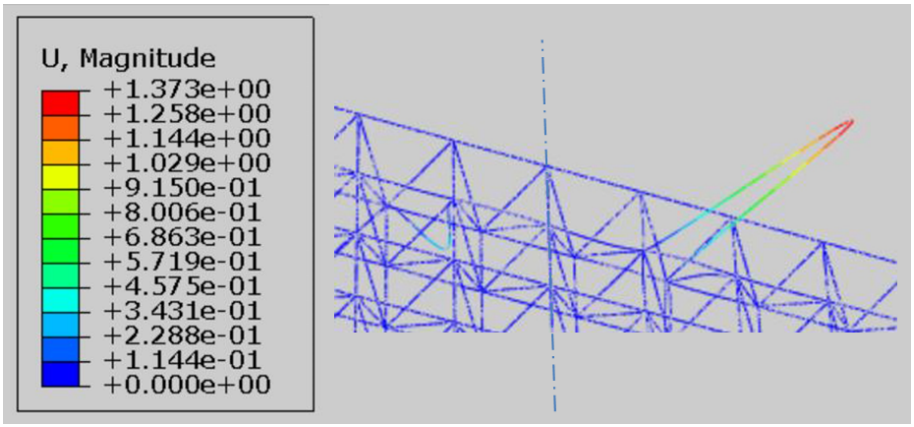

Figure 15. First buckling mode shape of the structure, located over the west facade.

Note that we restrict here our discussion to snow loads expressed in pressures, as pressure is the input parameter in the FE modelling. How those pressure levels can be interpreted in terms of depth and density of the snow cover on the roof will be presented further in the discussion part (see Section 4).

The results of the linear buckling analysis for a uniform pressure field are summarized in Table 5 and Figure 15. According to the analysis, buckling occurs locally. For each of the fourteen first eigenvalue modes, only two crossbars located on the

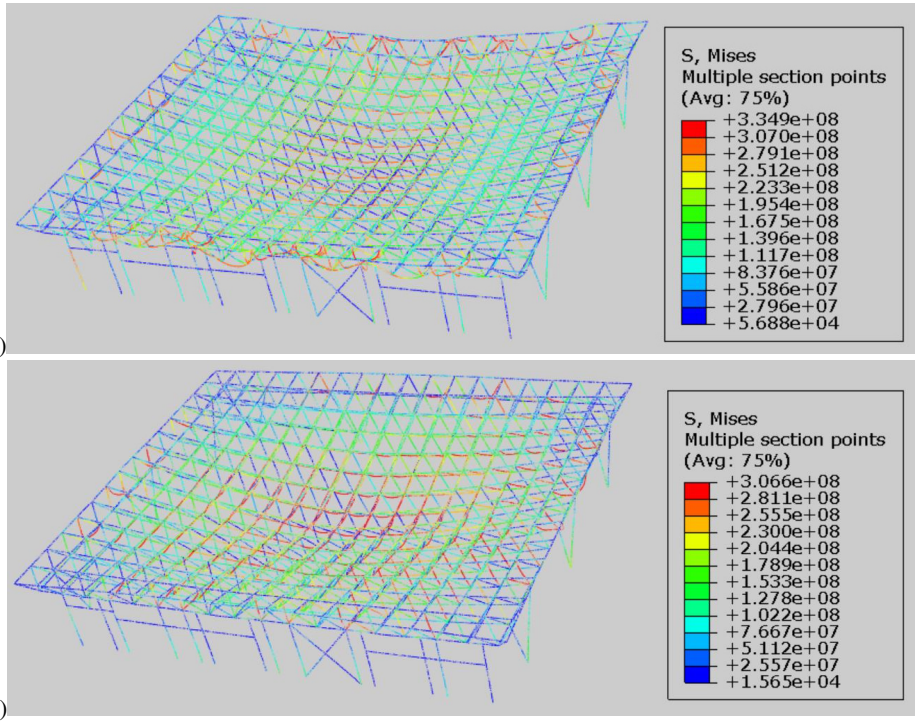

Figure 16. Von Mises stress field inside the structure at the last convergence step, given by the FE model simulation for a snow pressure field with (a) an accumulation on the sides and (b) a central accumulation.

perimeter of the roof buckle with a shape similar to the one of the first mode shown in Figure 15. Table 5 provides information about the buckling loads, displacements, and the location of crossbars prone to buckling for each eigenvalue mode. The table shows that buckling occurs first at the crossbars above the west facade and then above the east facade. Similar results are obtained for the other cases of snow-and-rain pressure distributions.

Figure 16 depicts the stress field of the structure at the last convergence step obtained by the pushover simulations in the cases of a pressure field with an accumulation on the sides and a central accumulation. In both cases, the maximum stresses occur at the bottom horizontal T-profiles located in the central part of the roof and at the crossbars located on the perimeter of the roof. In the case of a pressure field with accumulation on the sides, more crossbars on the perimeter of the roof, particularly above the west facade, yield and buckle, while more horizontal bars in the center of the roof yield in the case of a pressure field with a central accumulation. These results clearly indicate that failure occurred due to both buckling of the crossbars and bending of the bottom horizontal T-profiles. Other damage, such as those observed on the round tubular poles as shown in Figure A2c and A2d, likely occurred after, during the collapse of the structure. No such damage was observed on the nearby building, whereas slight buckling phenomena were identified on its roof. This subsequent damage was further modified by the presence of the offices and mezzanine walls along the north and south facades as shown in Figure A2e.

4 Discussion

This discussion section intends to make the link between the results from the snow and rain hazard (Section 2) and from the quasi-static pushover FE simulations (Section 3), in order to provide the most probable scenario which led to the collapse of the Irstea Cévennes building.

4.1 Building collapse analysis under the rain-on-snow event of February 2018

Figure 17 graphically summarizes the results of the quasi-static pushover and buckling FE simulations in the case of a uniform pressure distribution. Based on the hydrostatic pressure assumption ($\rho g h$), the iso-pressure curves corresponding to the different failure criteria used (see Table 4) can be plotted in the $(\rho, h)-$plane and this defines the safe and unsafe zones for the structure in terms of snowpack height h and density ρ. Below the dashed red-colored line (buckling limit), the structure remains intact. Above the continuous red-colored line (ultimate criterion), the structure collapses. In between (hatched zone in Figure 17), the structure undergoes irreversible damage that is more and more significant when approaching the continuous red-colored line. The dashed-dotted, dotted, and fine dashed-dotted red-colored lines define the yield limit, curvature limit based on the deflection of the structure, and horizontal displacement limit, respectively. Additionally, the buckling load obtained via the linear buckling analysis is represented by the fine dashed red-colored line.

The analysis of the chronicle of the climatic event described in Section 2 led to an initial snow depth on the ground (before rain) that certainly ranged from 30 to 35 cm and an initial snow density likely to be around 250 kg.m^{-3}. In this study, the snow load on the roof has been estimated to be equal to the snow load on the ground due to several reasons. Firstly, the roof slope was low, and a small wall was present around the edges of the roof. Secondly, the wind was not significant enough (force 1) to modify (reduce) the snow height on the roof. Lastly, no shape factor was used to estimate the snow load on the roof.

The corresponding two pairs of values (density ρ and height h, before rain) can be displayed in the $(\rho, h)-$plane of Figure 17, as depicted by the blue-colored triangles and circles. These two points can be directly compared to the iso-pressure curves inferred by the FE Abaqus simulations: they remain below the limits related to linear buckling, curvature, horizontal displacement, and material properties but are above the non-linear buckling limit that takes into account initial geometric imperfections (estimated to be 645 N.m^{-2}; see Table 4). They remain well below the load leading to the full collapse of the building, which is estimated to be $3\,410$ N.m^{-2}, as given by the ultimate limit criterion (see Table 4. Therefore, it can be safely concluded here that the initial snowfall (before rain) was critical for potential irreversible damage (buckling) to the structure, but it is unlikely to have been the sole cause of the full collapse.

As analysed in Section 2, the snowfall was followed by rain: during that rainfall, we consider that the snow cover density may have increased up to around 600 kg.m^{-3} due to partial saturation of the snowpack with water available. In reality, the wet snowpack was likely heterogeneous with areas of soared snow at higher densities (300-400 kg/m3) than the initial snow (250 kg/m3) and other areas at the bottom with accumulated water (1 000 kg/m3) due to preferential water flows. The value of 600 kg/m3 corresponds to an equivalent value used to define the (equivalent) pressure exerted by the combination of snow and rain accumulations. Predicting the evolution of the snowpack after rain and its interaction with the deforming structure is difficult

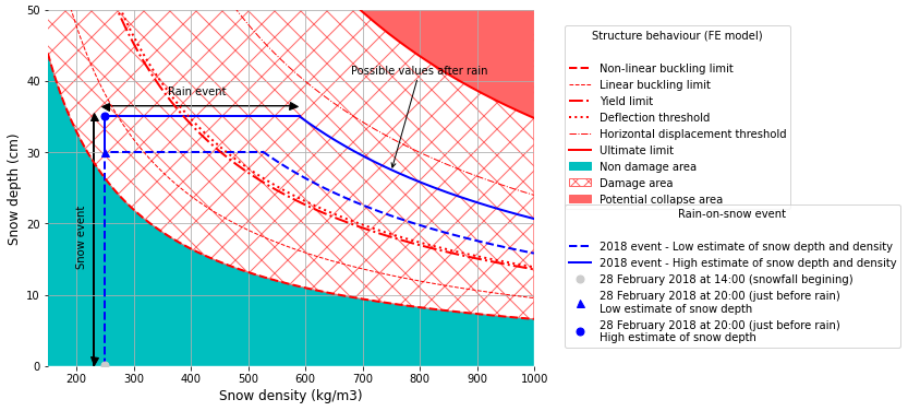

Figure 17. Comparison of the snow loads leading to different failure criteria of the Cévennes building, as calculated by FE model simulations, with different combinations of snow depth and density, assuming a uniform pressure field. The estimated scenario for the rain-on-snow event of 2018, as back-analyzed in Section 2, is also included in the comparison.

and we may expect some complicated dynamics that potentially produced a non-uniform pressure field during the rain event. In want of any monitoring or any full modeling of the snowpack evolution over time during the rain-on-snow event of 2018 and its interaction with the structure, we consider here one (simplified) scenario with no settling ($h = cste$) but a gradual increase of density due to water. This scenario is represented by the blue-colored horizontal lines drawn in Figure 17. Depending on the initial snow height and the ultimate limit reached for the density of the very wet snowpack after rain, this defines (ultimate) points that remain in the intermediate hatched zone for which the structure undergoes irreversible deformation. These points are still above safe limits in terms of buckling, yield, and deflection. As such, it can be concluded that the rain added to the snow cover initially in place certainly led to severe irreversible damage to the structure.

There are several sources of explanation for the fact that our analysis displayed on Figure 17 does predict irreversible damage but not a full collapse of the building. One reason is associated with the initial state of the structure which we assume as perfect with no previous damage experienced by the structure. An unknown initial damage which would have been taken into account in the FE simulatons could have easily brought the horizontal blue lines in the red zone. Another reason is that pushover simulations do not account for the buckling of the structure, while post-buckling analysis fails to predict the collapse of the structure.

4.2 Structural back analysis

In Appendix B, we discuss in detail the regulations: the one in place at the time of the construction of the Irstea Cevennes building and the one when the building collapse under snow load occurred. By comparing the regulations to the FE Abaqus calculations in terms of the applied stresses to the structure (see Figure B1 and related text in Appendix B), we show that the Irstea Cevennes building was correctly built in accordance with the previous French regulations (dating back to 1965), without accounting for any steel imperfections. We also conclude that the building, at the moment of its collapse in 2018, was

not respecting the new regulations; indeed, the critical buckling load of the structure (estimated at 645 N.m^{-2}), and the lower estimate of the load required to cause a deflection of 0.225 m (equal to $1\,205$ N.m^{-2}) were lower than the exceptional snow load specified in the Eurocode (equal to 0.8 x $1\,350 + 200 = 1\,280$ N.m^{-2}).

In this subsection, attention is paid to the identification of specific structural weaknesses which may have been critical, in so far as the FE simulations showed that structural weaknesses, combined with the extreme climatic event, can further explain the collapse.

Firstly, as indicated above, crossbars located at the perimeter of the lattice roof are clearly prone to buckling. Although this buckling is localized, it gradually weakens the structure and could potentially lead to its collapse. Similar phenomena were also observed after the 2018 incident on the nearby building.

Secondly, insofar as large-size vehicles (agricultural tractors) were to be used inside the building, no load-bearing walls were built inside. This led to the design of a very large span of the roof supporting lattice. Thus, our FE simulations suggest that the excessive deflection of the lattice is one cause of the collapse of the building under the rain-on-snow event of 2018. It should be noted that a neighbour building (see Figure 6), similar to the one which collapsed, resisted the event of February 2018 and is still in place on the site. This neighbour structure houses a number of offices and therefore includes some inner load-bearing walls. This may be an evidence that the latter walls inside the structure may be efficient to prevent significant deflections. This feedback could be considered in the future to encourage greater attention to the design of long-range roofs, particularly in the context of climate change leading which increases the uncertainties about the frequency and intensity of future rain-on-snow events.

Finally, the roof rain drainage system, consisting exclusively of vertical openings positioned in the lower part of the roof perimeter (see Figure 9), did not allow for the evacuation of rain once the roof was covered with snow. Indeed, significant water stagnation was observed on the roof of the similar nearby building a few days after the 2018 incident. Such a device thus led to a significant increase of the load supported by the lattice. This is another strongest structural weakness of the building, as evidenced by the following two scenarios considering no water evacuation, as depicted on the plots of Figure 17 (horizontal blue lines). In the future, it would be interesting to conduct more thorough studies of rainwater drainage on near-flat roofs during rain-on-snow events. It is important to clarify the effectiveness of various drainage solutions under snowy roof conditions, and to provide corresponding recommendations regarding the required roof slopes and the selection and design of downstream evacuation devices.

4.3 Characteristic snow loads in this region in a context of climate change

The rarity of large snow events at low elevations in this Mediterranean region makes the estimation of characteristic snow loads complex. Winters are generally mild in this area, with a low percentage of days below 0°C along the coasts. Significant snow events occur only every few years, and the high presence of zeros in the series makes the statistical treatment more difficult, as it is the case for low-latitude high-elevation zones (O'Donnell et al., 2020).

In a context of climate change, the French Mediterranean region, like most regions of the planet, is warming significantly (IPCC, 2021). Many studies have shown that extreme precipitation (snow and rain) events also intensify in this region

in past observations (Ribes et al., 2019) and according to climate projections (Tramblay and Somot, 2018). Concerning snow load extremes, future trends in this non-mountainous region are unclear, for several reasons:

- While extreme daily precipitation intensities are increasing, snow events become rarer as a result of global warming (snow events becoming rain events). It is not clear if extreme daily snow accumulations are decreasing if the occurrence of below-zero temperatures remains important.
- Climate models do not provide snow variables. While some studies provide projections of future snow conditions (e.g. Verfaillie et al., 2018), they are usually restricted to mountainous regions.
- Reports on the cryosphere generally focus on mountainous areas or high latitude areas (IPCC, 2019).

As a consequence, very few studies provide insights about past and future trends of snow loads in the region around Montpellier city. However, Croce and Landi (2021) recently show that characteristic snow loads are projected to increase along the coastlines of the French Mediterranean region. These results have important implications for current French standards, which have been established assuming 1/ a stationary climate (i.e. ignoring climate changes) 2/ a regional homogeneity, French standards being provided over large areas.

5 Conclusions

Using multiple sources of information regarding the 2018 meteorological event in terms of snow and rain amounts and detailed simulations of the behaviour of the roof structure subject to loads, this study provides a detailed back analysis of the interactions between the snow cover and the structure. Concerning the meteorological event, while intense snow events are unusual in this area, this type of event is not exceptional and occurs when winter storms bring important masses of cold air from northern Europe to the south (see the recent event in Madrid Smart, 2021). In Montpellier, snow depths around or above 30 cm have been recorded several times in the past (35 cm in February 1954, 35 cm during winter 1962-1963, 27 cm on the 14-16/01/1987, 28 cm on the 22/01/1992). For this event in Montpellier, the snow-rain transition led to a saturated and overweighted snowpack. A detailed understanding of the meteorological event has been consolidated using various sources of information: weather stations, numerical weather model outputs, meteorological reanalysis, and numerous testimonies obtained using social networks (facebook).

This study proposes an assessment of the response of the structure to the load under quasi-static conditions, as well as a buckling analysis. Different scenarios for distributions of the pressure field imparted to the structure have been studied, as both the behaviour of the snow cover during the rain-on-snow event and the response of the structure are transient and non-uniform processes, for which the properties evolve gradually over time and space. Based on the results obtained, the collapse of the Irstea Cévennes building can be explained by two main factors. Firstly, the structure was weak against buckling and bending, despite being designed in accordance with the regulations at the time it was built. Secondly, the collapse may have been contributed to by the intensity of the rain-on-snow event, as well as the fact that the rainwater was unable to flow due to

the low slope of the roof and the small 20 cm drainage openings. These openings were likely blocked by the dense snowpack that had already accumulated when the precipitation turned into rain. Thus, it is evident that geometric imperfections were not considered during the design of the structure, resulting in its vulnerability to buckling. Moreover, the snow cover started saturating and the resulting load exceeded the critical load leading to roof failure. Such a rain-on-snow scenario is considered in the regulations but it appears that in the particular chronicle of the 2018 event (significant amounts of snow and then of water with varying temperature conditions) the resulting overload was greater than the design scenario.

In conclusion, this study has shown that some older metallic buildings, whose design did not take into account imperfections, may be at risk of buckling during exceptional rain-on-snow events. Additionally, inadequate rainwater drainage can also enhance this risk. Therefore, it would be interesting to conduct research in the near future to determine the effectiveness of different rainwater drainage systems for relatively flat roofs where a high level of snow accumulation can occur during snow events followed by intense rainfall. This would facilitate the development of recommendations on the subject in the future.

The evolution of intense snow events, in a context of climate change, is particularly unclear because of concurrent factors. While precipitation extremes are expected to intensify in this region (Tramblay and Somot, 2018), we expect more precipitation events falling as rain instead of snow in this region. However, climate models simulate important changes in the dynamics of these events, and very few studies (at the exception of Croce and Landi, 2021) assess extreme snow events in non-mountainous regions.

Author contributions

TF coordinated and supervised the back-analysis study. GE and DR performed the analysis of the meteorological event. IO carried out the FE model simulations of the loaded building and proposed a first comparison between the FE simulations' results and the analysis of the snow and rain hazard. All authors discussed the results and co-wrote the manuscript.

Competing interests

The authors declare that they have no conflict of interest.

Acknowledgements

The authors thank Mohamed Naaim for having motivated this research. They are grateful to Meteo-Languedoc and Meteociel for sharing the meteorological information and resources. They also thank Jean-Luc Descrismes and Sylvain Labbé of INRAE for having provided all available information about the Irstea Cévennes building.

Figure A1. Location map of the Irstea Cévennes building in Montpellier. Source: Inrae.

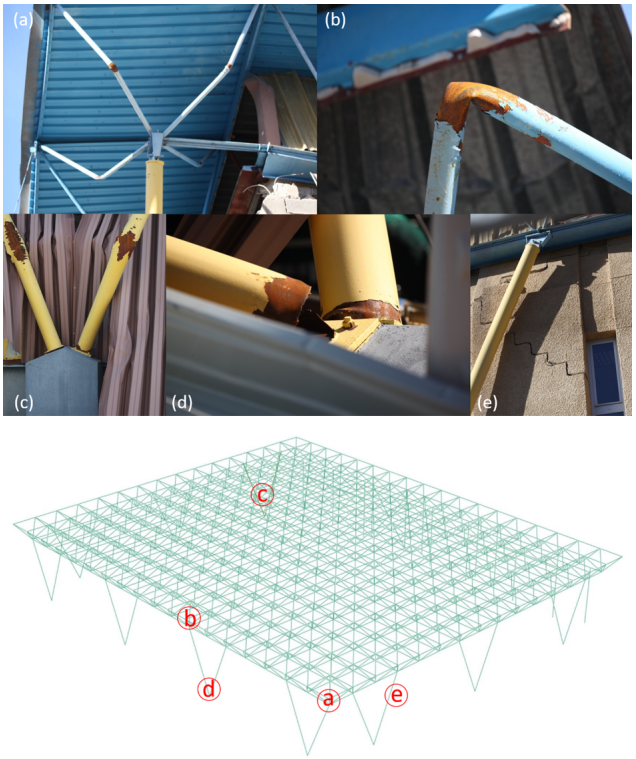

Figure A2. Close-up views of damage to the structure of the Irstea Cévennes hall, as observed on March 18, 2018: buckling and bending failure of roof tubular profiles (a,b), bending and shear failures of tubular supporting pylons (c,d) and cracking of the inner offices' walls made of concrete and located along the southern face of the building.

Appendix A: Additional information about the Irstea Cévennes building

This appendix gives some details about the Irstea Cévennes building, in addition to the information already provided in the main text (Section 3).

Figure A1 provides the location map of the Cévennes building in the Montpellier site of Irstea (now INRAE).

Figure A2 gives close-up views of the different types of damage to the structure of the Irstea Cévennes building, as observed on March 18, 2018, a couple of weeks after the roof collapse.

Figure A3 gives a description of the geometry of the metal structure modelled by FE Abaqus software, including the details of the geometry of each component. The numerical values given to the different geometrical properties defined in Figure A3 are given in Table A1.

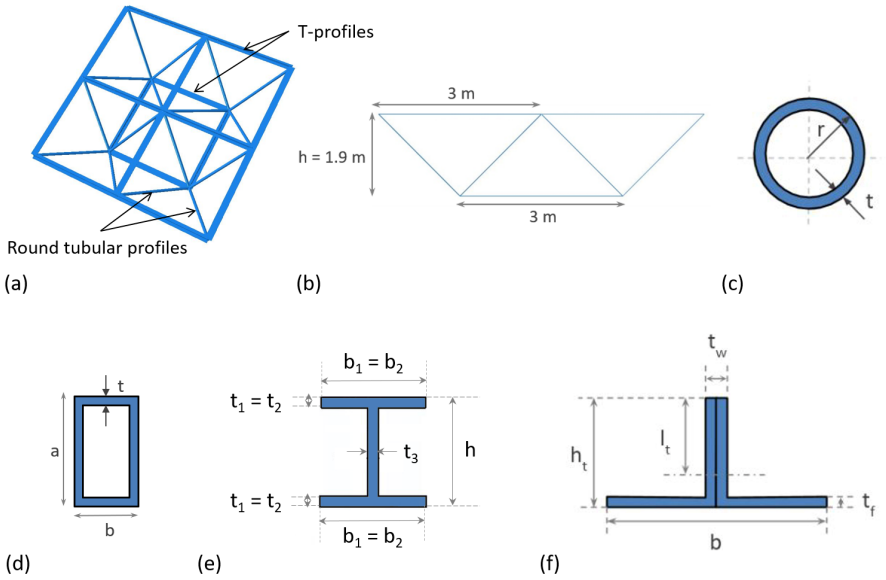

Figure A3. Details of the metal structure modelled by the FE Abaqus software: general view (a) and front view of one single roof frame element (b), round (c), and rectangular (d) tubular profiles' and HEA (e) and T- (f) profiles' features.

Appendix B: Analysis of the building collapse considering the regulations

The existing regulation for engineering snow load design in France at the time of the Irstea building construction in 1982 was the French standard which defines the snow and wind effects on construction, initially published in 1965 (CGNG, 2000). This French standard was based on geographical areas (regions I, II, III and a region III + 45%) for which snow loads on floor below 200 m above sea level were defined *a priori*. Table B1 gives the values of ground snow loads which had to be taken into account to design buildings located in the region II including Montpellier city.

Today, in compliance with Eurocode 1 and the NF EN 1991-1-3 standard adopted in France according to Eurocode 1 (CEN/TC250, 1991; AFNOR, 2004, 2007), snow load on a roof, s, is defined by the following equation:

$$s = \mu_i \cdot C_e \cdot C_t \cdot s_o, \tag{B1}$$

where $s_o = s_k$ or s_{Ad}, and where s_k and s_{Ad} are the ground snow loads for permanent/transitional and accidental project situations, respectively (with respect to the geographical zone under consideration). μ_i represents the roof shape coefficient that accounts for undrifted and drifted snow load arrangements, respectively, depending on the shape and the slope of the roof. C_e is the exposure coefficient (equal to 0.8 for a windswept site, 1 for a normal site and 1.25 for a sheltered site). C_t is the thermal coefficient (equal to 1 for a roof that has no high thermal transmittance).

Ground snow load values to be used in France are given for eight different zones depending on the altitude (those concerned by the present case are referred in Table B2). They are determined on the basis of a probability that they will be exceeded over

Table A1. Geometrical properties of the structure

Parameter	Symbol	Value	Unit
Global structure			
Roof wide	l	45.00	m
Roof length	L	54.00	m
Roof height	h	1.90	m
Total height	H	9.90	m
Top and (bottom) roof lattice T-profiles			
Wide	b	160 (120)	mm
Height	h_t	100 (80)	mm
Thickness	t_f	9 (7)	mm
Thickness	t_w	18 (14)	mm
Position of the local cross-section axis	l_t	68.9 (54.5)	mm
HEA 160			
Wide	$b_1 = b_2$	160	mm
Height	h	152	mm
Thickness	$t_1 = t_2$	9	mm
Thickness	t_w	6	mm
Round tubular profiles of roof lattice			
Outer radius	r	24.15	mm
Thickness	t	2.9	mm
Round tubular profiles of facades			
Outer radius	r	109.55	mm
Thickness	t	4.5	mm
Rectangular tubular profiles			
Height	a	100	mm
Wide	b	50	mm
Thickness	t	2	mm

Table B1. Values of ground snow load [N.m^{-}2] to be considered according to the French NV65 standard published in 1965 for the region II where Montpellier city is located.

Region	II
Normal overload	450
Extreme overload	750

a one-year period (excluding the case of exceptional snow) equal to 0.02 and assuming a snow density of 150 kg.m^{-3}. Note that such a value for density corresponds to relatively dry and fresh snow and remains well below the typical density of humid snow (around 250 kg.m^{-3}), as involved in the present case study which concerns a Mediterranean area (see Section 2).

Table B2. Values of ground snow load [N.m^{-2}] for the region where Montpellier city is located according to the NF EN 1991-1-3 standard published in 1991.

Region	B2
Characteristic value of ground snow load (s_k)	
at an altitude of less than 200 m	550
Design value of exceptional ground snow load (s_{Ad})	1 350

Eurocode 1 also provides that in areas where rain on snow may cause melting followed by frost, snow loads on roof must be increased, especially if snow and ice can block the roof drainage system. The NF EN 1991-1-3 standard stipulates that roof snow load must be increased by 0.2 kN.m^{-2} when the slope for water flow is lower than 3 %, in order to account for the snow density increase resulting from difficulties of water drainage in case of rain.

In our case, the roof of the building being made of one single slope that is less than $30°$, only one load case is to be considered in permanent project situation and $\mu_i = \mu_1 = 0.8$ for both permanent and accidental project situations with typical and exceptional snow loads, respectively.

So, in Figure B1, roof snow loads leading to the failure criteria of the Cévennes supporting structure according to the FE model simulations in the most critical case of pressure field with a central accumulation (in the range $645 - 1\,915$ N.m^{-2} for criteria other than the ultimate limit) are compared to values (without safety factors) recommended by the French DTU NV65 standard, valid at the moment of the building construction in 1982 (450 and 750 N.m^{-2} for normal and extreme design loads) and the NF EN 1991-1-3 standard, adopted in application of Eurocode 1 ($0.8 * 550 + 200 = 640$ and $0.8 * 1\,350 + 200 = 1\,280$ N.m^{-2} for characteristic and exceptional design loads, respectively).

In France, the consideration of imperfections in the design of metallic structures was introduced in the regulations in 1983, with the publication of the first version of the Regulation on Metal Construction, so after the construction of the building studied here. If initial geometric imperfections are not taken into account (linear buckling limit), and even more if the dead load of the structure is neglected in the estimation of the critical buckling load (linear buckling limit without dead weight), the results show that the structure begins to be damaged by snow loads (equal to 940 and 1 235 kN.m^{-2}, respectively) largely above the normal and extreme loads recommended by the DTU NV65, which are 450 and 750 kN.m^{-2}. It seems, therefore, that the design of this building was executed in accordance with the state of the art at that time.

Under current regulations, taking into account initial geometric imperfections, buckling occurs first for a load of 645 N.m^{-2} which is of the same order of magnitude as the characteristic design load (that corresponds to a snow load equal to 640 N.m^{-2}) and well below the exceptional load (equal to $1\,280$ N.m^{-2}) recommended by Eurocode. Moreover, in the case of a central accumulation of snowpack, the building fails serviceability (excessive deflection) for a load of 1 205 N.m^{-2} just less than the exceptional load recommended by Eurocode. It is therefore clear that this structure was not consistent with the current design basis rules. In contrast, the building begins to yield and fails serviceability from a horizontal displacement point of view for

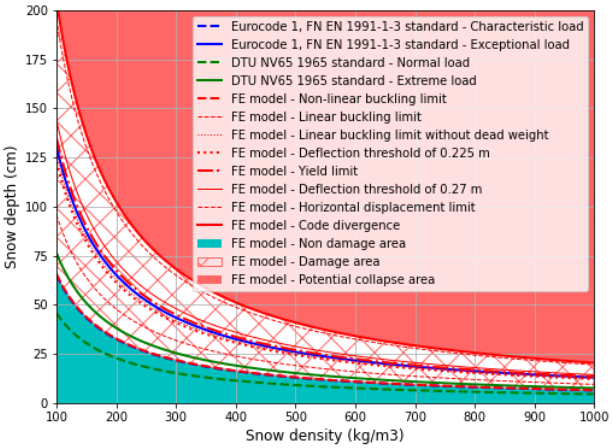

Figure B1. Comparison for different combinations of snow depth and density between the snow loads leading to the different failure criteria of the Cévennes building, as calculated by the FE model, and the snow load values recommended by Eurocode 1 and the DTU NV65 without taking into account safety factors (both in terms of loads and the steel behaviour law) in the case of a snow pressure field with a central accumulation.

snow loads (equal to 1325 and 1925 N.m^{-2} respectively) largely above the characteristic project situation and above this exceptional load too.

References

AFNOR: NF EN 1991-1-3 : Eurocode 1 : Actions sur les structures - Partie 1-3 : Actions générales - charges de neige, Association Francaise de Normalisation (AFNOR), 2004.

AFNOR: NF EN 1991-1-3/NA : Eurocode 1 : Actions sur les structures - Partie 1-3 : Actions générales - charges de neige. Annexe nationale à la NF EN 1991-1-3, Association Francaise de Normalisation (AFNOR), 2007.

Altunişik, A., Ateş, S., and Hüsem, M.: Lateral buckling failure of steel cantilever roof of a tribune due to snow loads, Engineering Failure Analysis, 72, 67–78, https://doi.org/10.1016/j.engfailanal.2016.12.010, 2017.

Biegus, A. and Kowal, A.: Collapse of halls made from cold-formed steel sheets, Engineering Failure Analysis, 31, 189–194, https://doi.org/10.1016/j.engfailanal.2012.12.009, 2013.

Biegus, A. and Rykaluk, K.: Collapse of Katowice Fair Building, Engineering Failure Analysis, 16, 1643–1654, https://doi.org/10.1016/j.engfailanal.2008.11.008, 2009.

Bouttier, F. and Roulet, B.: Arome, the new high resolution model of Meteo-France, The European forecaster - Newsletter of the WGCEF (Printed by Meteo-France), 13, 27–30, 2008.

Brencich, A.: Collapse of an industrial steel shed: A case study for basic errors in computational structural engineering and control procedures, Engineering Failure Analysis, 17, 213–225, https://doi.org/10.1016/j.engfailanal.2009.06.015, 2010.

Caglayan, O. and Yuksel, E.: Experimental and finite element investigations on the collapse of a Mero space truss roof structure – A case study, Engineering Failure Analysis, 15, 458–470, https://doi.org/10.1016/j.engfailanal.2007.05.005, 2008.

CEN/TC250: Eurocode 1: Actions on structures - Part 1-3: General actions - Snow loads (EN 1991-1-3), Comité européen de Normalisation / Comité Technique CEN/TC 250 "Eurocodes structuraux", 1991.

CGNG: Règles NV 65, modifiées en décembre 1999, avril 2000 et février 2009 et annexes. DTU P 06-002 : Règles définissant les effets de la neige et du vent sur les constructions., Commission Générale de Normalisation du Bâtiment, 2000.

Croce, P.and Formichi, P. and Landi, F.: Extreme Ground Snow Loads in Europe from 1951 to 2100, Climate, 9, 133, https://doi.org/10.3390/cli9090133, 2021.

Dassault Systèmes: Abaqus/Standard. Version 11.2., Tech. rep., Providence, RI: Dassault Systèmes Simulia Corp., 2017.

del Coz Díaz, J., Álvarez Rabanal, F., García Nieto, P., Roces-García, J., and Alonso-Estébanez, A.: Nonlinear buckling and failure analysis of a self-weighted metallic roof with and without skylights by FEM, Engineering Failure Analysis, 26, 65–80, https://doi.org/10.1016/j.engfailanal.2012.07.019, 2012.

Geis, J., Strobel, K., and Liel, A.: Snow-Induced Building Failures, Journal of Performance of Constructed Facilities, 26, 377–388, https://doi.org/10.1061/(ASCE)CF.1943-5509.0000222, 2012.

Geis, J. M.: The Effects of Snow Loading on Lightweight Metal Buildings with Open-Web Steel Joists, Master's thesis, University of Colorado, http://localhost/files/n583xv25x, 2011.

Holický, M. and Sýkora, M.: Failures of Roofs under Snow Load: Causes and Reliability Analysis, American Society of Civil Engineers, pp. 444–453, https://doi.org/10.1061/41082(362)45, 2009.

IPCC: Special Report on the Ocean and Cryosphere in a Changing Climate, [h.-o. portner, d.c. roberts, v. masson-delmotte, p. zhai, m.602 tignor, e. poloczanska, k. mintenbeck, a. alegra, m. nicolai, a. okem, j.603 petzold, b. rama, n.m. weyer (eds.)], 2019.

IPCC: Climate Change 2021: The Physical Science Basis. Contribution of Working Group I to the Sixth Assessment Report of the Intergovernmental Panel on Climate Change, [Masson-Delmotte, V., P. Zhai, A. Pirani, S.L. Connors, C. Péan, S. Berger, N. Caud, Y. Chen, L.

Goldfarb, M.I. Gomis, M. Huang, K. Leitzell, E. Lonnoy, J.B.R. Matthews, T.K. Maycock, T. Waterfield, O. Yelekçi, R. Yu, and B. Zhou (eds.)], Cambridge University Press, 2021.

Krentowski, J., Chyzy, T., Dunaj, P., and Dunaj, P.: Delayed catastrophe of a steel roofing structure of a shopping facility, Engineering Failure Analysis, 98, 72–82, https://doi.org/10.1016/j.engfailanal.2019.01.082, 2019.

Le Roux, E., Evin, G., Eckert, N., Blanchet, J., and Morin, S.: Non-stationary extreme value analysis of ground snow loads in the French Alps: a comparison with building standards, Natural Hazards and Earth System Sciences, 20, 2961–2977, https://doi.org/10.5194/nhess-20-2961-2020, 2020.

Marshall, H.-P., Conway, H., and Rasmussen, L.-A.: Snow densification during rain, Cold Regions Science and Technology, pp. 35–41, 1999.

O'Rourke, M. and Wikoff, J.: Snow-Related Roof Collapse during the winter of 2010-2011: Implications for Building Codes, American Society of Civil Engineers, https://doi.org/10.1061/9780784478240, 2014.

O'Donnell, F., Tingerthal, J., and White, S.: Estimation of Ground Snow Loads for Low-Latitude, High-Elevation Regions, Journal of Cold Regions Engineering, 34, 04020 008, https://doi.org/10.1061/(ASCE)CR.1943-5495.0000209, 2020.

Piroglu, F. and Ozakgul, K.: Partial collapses experienced for a steel space truss roof structure induced by ice ponds, Engineering Failure Analysis, 60, 155–165, https://doi.org/10.1016/j.engfailanal.2015.11.039, 2016.

Piskoty, G., Wullschleger, L., Loser, R., Herwig, A., Tuchschmid, M., and Terrasi, G.: Failure analysis of a collapsed flat gymnasium roof, Engineering Failure Analysis, 35, 104–113, https://doi.org/10.1016/j.engfailanal.2012.12.006, special issue on ICEFA V- Part 1, 2013.

Ribes, A.and Thao, S., Vautard, R.and Dubuisson, B., Somot, S., Colin, J., Planton, S., and Soubeyroux, J.-M.: Observed increase in extreme daily rainfall in the French Mediterranean, Climate Dynamics, 52, 1095–1114, https://doi.org/10.1007/s00382-018-4179-2, 2019.

Smart, D.: Storm Filomena 8 January 2021, Weather, 76, 98–99, https://doi.org/10.1002/wea.3950, 2021.

Strasser, U.: Snow loads in a changing climate: New risks?, Natural Hazards and Earth System Sciences, 8, https://doi.org/10.5194/nhess-8-1-2008, 2008.

Tramblay, Y. and Somot, S.: Future evolution of extreme precipitation in the Mediterranean, Climatic Change, 151, 289–302, https://doi.org/10.1007/s10584-018-2300-5, 2018.

Verfaillie, D., Lafaysse, M., Déqué, M., Eckert, N., Lejeune, Y., and Morin, S.: Multi-component ensembles of future meteorological and natural snow conditions for 1500 m altitude in the Chartreuse mountain range, Northern French Alps, The Cryosphere, 12, 1249–1271, https://doi.org/10.5194/tc-12-1249-2018, 2018.

Vidal, J.-P., Martin, E., Franchistéguy, L., Baillon, M., and Soubeyroux, J.-M.: A 50-year high-resolution atmospheric reanalysis over France with the Safran system, International Journal of Climatology, 30, 1627–1644, https://doi.org/10.1002/joc.2003, 2010.

Winter, S. and Kreuzinger, H.: The Bad Reichenhall ice-arena collapse and the necessary consequences for wide span timber structures, in: 10th World Conference on Timber Engineering, vol. 4, pp. 1978–1985, Miyazaki, Japan, 2008.